Research Article Vol. 8, No. 9 / September 2021 / Optica 1219

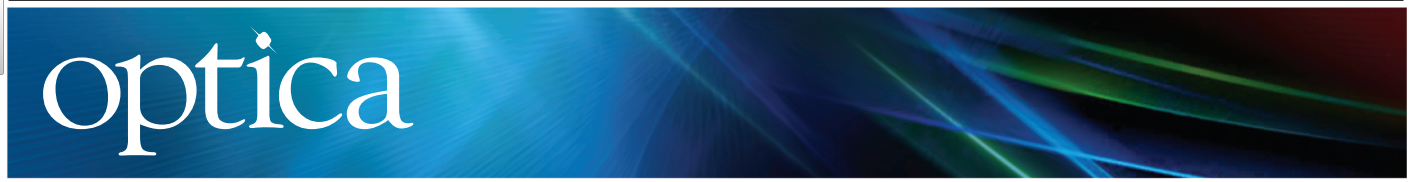

Nonlinear enhanced microresonator gyroscope

Jonathan M. Silver,[1,*] Leonardo Del Bino,[2] Michael T. M. Woodley,[3] George N. Ghalanos,[2,3] Andreas Ø. Svela,[3] Niall Moroney,[3] Shuangyou Zhang,[2] Kenneth T. V. Grattan,[4] and Pascal Del'Haye[2,5,6]

[1]National Physical Laboratory, Hampton Road, Teddington TW11 0LW, UK
[2]Max Planck Institute for the Science of Light, 91058 Erlangen, Germany
[3]Imperial College London, London SW7 2AZ, UK
[4]City, University of London, Northampton Square, London EC1V 0HB, UK
[5]Department of Physics, Friedrich–Alexander University Erlangen–Nuremberg, 91058 Erlangen, Germany
[6]e-mail: pascal.delhaye@mpl.mpg.de
*Corresponding author: jonathan.silver@npl.co.uk

Received 24 March 2021; revised 10 June 2021; accepted 11 June 2021 (Doc. ID 426018); published 17 September 2021

Optical gyroscopes based on the Sagnac effect have been the mainstay of inertial navigation in aerospace and shipping for decades. These gyroscopes are typically realized either as ring-laser gyroscopes (RLGs) or fiber-optic gyroscopes (FOGs). With the recent rapid progress in the field of ultrahigh-quality optical whispering-gallery mode and ring microresonators, attention has been focused on the development of microresonator-based Sagnac gyroscopes as a more compact alternative to RLGs and FOGs. One avenue that has been explored is the use of exceptional points in non-Hermitian systems to enhance the responsivity to rotation. We use a similar phenomenon, namely, the critical point of a spontaneous symmetry-breaking transition between counterpropagating light, to demonstrate a microresonator gyroscope with a responsivity enhanced by a factor of around 10^4. We present a proof-of-principle rotation measurement as well as a characterization of the system's dynamical response, which shows the universal critical behaviors of responsivity enhancement and critical slowing down, both of which are beneficial in an optical gyroscope. We believe that this concept could be used to realize simple and cheap chip-based gyroscopes with sensitivities approaching those of today's RLGs and FOGs.

https://doi.org/10.1364/OPTICA.426018

1. INTRODUCTION

The ultrahigh quality (Q) factors achievable with optical microresonators offer the possibility of realizing a novel form of an optical gyroscope [1,2] with a fraction of the size, weight, power consumption, and cost of fiber-optic gyroscopes (FOGs) and ring-laser gyroscopes (RLGs) [1]. Advances in microfabrication techniques, combined with innovative methods of measuring the Sagnac effect [3] in microresonators, are beginning to make mass-producible, chip-based optical gyroscopes a real possibility. Examples of such methods include phase modulation schemes [4,5], the Pound–Drever–Hall (PDH) technique [6], and stimulated Brillouin scattering or lasing [7–9]. Several techniques for enhancing the rotation sensitivity have been proposed and demonstrated, including phase difference traversal [10], dual-resonator reciprocal measurement [11], tunable dispersion [12], and the use of exceptional points (EPs) in non-Hermitian systems [8,13,14]. This last example has attracted considerable interest, as the response of the resonator is proportional to the square root of the rotation velocity at an EP, potentially leading to a sensitivity increase of several orders of magnitude. Indeed, a four-fold increase in responsivity has been observed using an EP [8]. However, recent work has also shown that despite the divergent responsivity at an EP, the fundamental sensitivity limit does not markedly increase in these systems, since some of the noise from both quantum and other sources is amplified by the same factor as the signal [15–18], although instabilities due to parametric noise can be removed at the cost of reducing sensitivity [19]. The most sensitive microresonator gyroscopes reported so far, with bias drifts of 3 deg/h [6] and 3.6 deg/h [9], do not use EPs for reponsivity enhancement, but rather focus on achieving a low noise floor.

One of the key features of ultrahigh-Q optical microresonators is the strong Kerr nonlinearity that they exhibit at modest input powers of milliwatts or even microwatts, leading to important effects such as frequency comb generation [20–22]. Recently, Kerr interaction between counterpropagating light waves in a bidirectionally pumped microresonator was found to give rise to spontaneous symmetry breaking [23–25]. This occurs because the Kerr interaction between the counterpropagating waves, a form of cross-phase modulation, is stronger than self-phase modulation by a factor of 2 in a dielectric solid, which means that differences between the counterpropagating circulating powers self-amplify via resonance frequency splittings and consequent pump-resonance detuning differences. As well as enabling novel nonreciprocal optical components [26] and optical memories [27], this symmetry breaking drastically enhances the response of the

resonator to rotation [28,29] and near-field perturbations [30,31]. This occurs when the system is operating close to the critical point of the symmetry-breaking transition, with a cube-root response, and hence divergent responsivity to small rotation velocities, at the critical point itself. Divergent sensitivity to external perturbations is actually a universal feature of critical points in general [32], occurring in systems as diverse as the Higgs mechanism [33], ferromagnetism, liquid–gas critical points, superconductivity [34], and superfluidity [35]. Another such universal feature is critical slowing down [32], where the characteristic timescale of the system's response to a perturbation diverges towards the critical point.

Based on this principle, we demonstrate an enhanced gyroscope using a silica microrod resonator [36] with diameter 2.8 mm and $Q = 2.9 \times 10^8$ coupled to a tapered optical fiber pumped with laser light at 1550 nm. We directly observe both responsitivity enhancement and critical slowing down. Both of these effects are beneficial for a gyroscope, as together they cause the system to act like a single-pole low-pass filter with a cutoff frequency that approaches zero the closer the system is to the critical point [37]. In other words, the system takes an amplified moving average of the rotation velocity over a timescale equal to the inverse of the cutoff frequency and above this frequency behaves like an integrator. This is in particular useful for inertial navigation in vehicles such as aircraft and spacecraft that only rotate slowly.

2. THEORETICAL BACKGROUND

In an optical ring resonator of diameter D and refractive index n_0 rotating in its plane at angular velocity Ω, the Sagnac effect causes the resonance frequencies of counterpropagating pairs of modes at vacuum wavelength λ to differ by an amount [3]

$$\Delta\omega = 2\pi \frac{D\Omega}{n_0\lambda}. \tag{1}$$

For 1550 nm light in a silica resonator with a diameter of a few millimeters, rotating at 1 deg/s, this is just tens of hertz (Hz), which is already 3–4 orders of magnitude smaller than the resonator's linewidth, even for a state-of-the-art Q factor of 10^9 [38]. Thus, to turn such a resonator into a gyroscope that significantly improves on microelectromechanical systems (MEMS) devices [39], it is necessary to be able to detect splittings of $<10^{-5}$ of the linewidth, which, although challenging, has actually been achieved using the PDH technique [6].

Here, we investigate how the responsivity enhancement [28,29] that exists near the critical point of Kerr-mediated symmetry breaking between counterpropagating light fields [23,25] may be used to measure Sagnac splittings several orders of magnitude smaller than the resonator's linewidth with a potentially very simple setup, as illustrated in Fig. 1(a). Monochromatic light of the same power and frequency is coupled evanescently into a high-Q ring resonator in both the clockwise and counterclockwise directions. The pump power and detuning are chosen so as to place the resonator close to the critical point of the symmetry breaking.

Throughout this text, we shall express quantities in the dimensionless forms listed in Table 1. Time is normalized by the inverse half-linewidth $1/\gamma$ and angular frequencies by γ. Since the dynamics we are interested in take place over timescales much longer than $1/\gamma$, cavity ringdown effects are negligible, meaning that the values of the circulating powers $p_{1,2}$ are directly related to

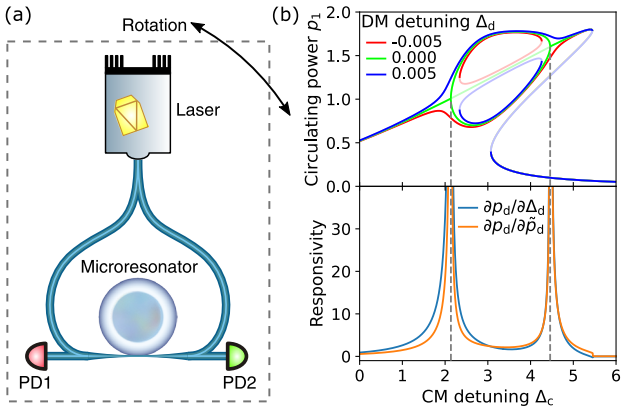

Fig. 1. (a) Simplified schematic of the nonlinear enhanced microresonator gyroscope. A high-Q optical ring resonator is pumped equally in both directions with narrow-linewidth continuous-wave laser light via a tapered optical fiber. The power and detuning are set so as to place the resonator near the critical point of the symmetry-breaking regime [23,25], and the transmitted powers, indicative of the circulating powers, are detected on two photodiodes (PD). Rotation in the plane of the resonator causes a difference between the readings on PD1 and PD2. (b) Top: Circulating power p_1 in one of the two directions versus common-mode (CM) detuning Δ_c for three values of the differential-mode (DM) detuning Δ_d and equal pump powers $\tilde{p}_{1,2} = 1.8$ (see Table 1). The way in which the blue, green, and red curves deviate significantly from one another approaching the critical points (of which we use the left one in the experiments) is indicative of the system's divergent responsivity to Δ_d. All quantities are in their dimensionless forms (see Table 1). Faint lines correspond to unstable solutions. By symmetry, the curves for p_2 are identical but with Δ_d negated, so when p_1 takes the upper blue curve p_2 takes the lower red one, etc. Bottom: Partial derivatives of the DM circulating power p_d with respect to the DM detuning Δ_d and pump power $\tilde{p}_d$ for the stable solutions in the case $\Delta_d = 0$. These are calculated using Eqs. (S1) and (S2) in Supplement 1, which are equivalent to Eqs. (5) and (6) in the symmetry-unbroken regions where $p_d = 0$.

the transmitted powers detected on the photodiodes (PDs) in the counterpropagating directions (see Fig. 1).

In the steady state, $p_{1,2}$ obey the following pair of simultaneous equations [37]:

$$p_{1,2} = \frac{\tilde{p}_{1,2}}{1 + (p_{1,2} + 2p_{2,1} - \Delta_{1,2})^2}. \tag{2}$$

Note the factor of 2 in front of the counterpropagating circulating power, which represents the ratio between the strengths of cross- and self-phase modulation. For symmetric pump powers $\tilde{p}_{1,2} = \tilde{p}$ and detunings $\Delta_{1,2} = \Delta$, the symmetric solution $p_{1,2} = p$ thus satisfies

$$p = \frac{\tilde{p}}{1 + (3p - \Delta)^2}. \tag{3}$$

For $\tilde{p}$ above the threshold $8/(3\sqrt{3}) \simeq 1.54$, a symmetry-broken regime exists, in which the symmetric solution is unstable and is replaced by two stable asymmetric solutions that map to each other under swapping of the two directions. The critical points satisfy the condition [37]

$$(p - \Delta)(3p - \Delta) = -1. \tag{4}$$

This symmetry breaking is illustrated in Fig. 1(b) for $\tilde{p} = 1.8$. The upper panel shows how a detuning difference of just 1% of

Table 1. Dimensionless Quantities Used in this Paper[a]

x	Description	Formula
$\tilde{p}_{1,2}$	Pump powers	$\eta_{\text{in}} P_{\text{in},1,2}/P_0$
$p_{1,2}$	Circulating powers	$2\pi P_{\text{circ},1,2}/(\mathcal{F}_0 P_0)$
$\Delta_{1,2}$	Pump detunings from resonance frequency without Kerr shift	$(\omega_0 - \omega_{1,2})/\gamma$
$\tilde{e}_{1,2}$	Pump field amplitudes	$\tilde{p}_{1,2} = \lvert\tilde{e}_{1,2}\rvert^2$
$e_{1,2}$	Circulating field amplitudes	$p_{1,2} = \lvert e_{1,2}\rvert^2$
$\epsilon_{1,2}$	Fractional pump power perturbations	$\tilde{p}_{1,2} = \tilde{p}(1+\epsilon_{1,2})$
$\tilde{p}_{\text{c,d}}$, $p_{\text{c,d}}$, $\Delta_{\text{c,d}}$, $\epsilon_{\text{c,d}}$	CM and DM components	For $X \in \{\tilde{p}, p, \Delta, \epsilon\}$, $X_{\text{c}} = (X_1 + X_2)/2$, $X_{\text{d}} = (X_1 - X_2)/2$
δ_{c}	CM pump detuning offset from critical point	$\Delta_{\text{c}} - \Delta$

[a]The subscripts 1 and 2 refer to the two counterpropagating directions, and 'c' and 'd' to common- and differential-mode (CM and DM) combinations of these. η_{in} is the resonant in-coupling efficiency equal to $4\kappa\gamma_0/\gamma^2$, where κ, γ_0, and $\gamma = \gamma_0 + \kappa$ are the coupling, intrinsic, and total half-linewidths, respectively. $P_{\text{in},1,2}$ and $P_{\text{circ},1,2}$ are the pump and circulating powers, respectively. $P_0 = \pi n_0^2 V/(n_2 \lambda Q Q_0)$ is the characteristic in-coupled power required for Kerr nonlinear effects, where n_0 and n_2 are the linear and nonlinear refractive indices, V is the mode volume, and $Q = \omega_0/(2\gamma)$ and $Q_0 = \omega_0/(2\gamma_0)$ are the loaded and intrinsic Q factors, respectively, for cavity resonance frequency ω_0 (without Kerr shift). $\mathcal{F}_0 = \Delta\omega_{\text{FSR}}/(2\gamma_0)$ is the cavity's intrinsic finesse for free spectral range $\Delta\omega_{\text{FSR}}$, $\omega_{1,2}$ are the two pump frequencies, and Δ is the value of $\Delta_1 = \Delta_2$ at the critical point.

the half-linewidth causes the two circulating powers to differ by a large proportion near the critical points. The responsivity in fact diverges as the critical point is approached, as shown in the lower panel, which makes the system useful as a gyroscope, since rotation is directly linked to Δ_{d}. However, the system is simultaneously divergently responsive to differences in pump power, which means that the sensitivity to rotation is limited by the stability of the pump power difference. These responsivities, for $\tilde{p}_{\text{d}} = p_{\text{d}} = \Delta_{\text{d}} = 0$, are given by

$$\frac{\partial p_{\text{d}}}{\partial \Delta_{\text{d}}} = \frac{1}{1 + (p_{\text{c}} - \Delta_{\text{c}})(3p_{\text{c}} - \Delta_{\text{c}})}, \tag{5}$$

$$\frac{\partial p_{\text{d}}}{\partial \tilde{p}_{\text{d}}} = \frac{2p_{\text{c}}(3p_{\text{c}} - \Delta_{\text{c}})}{1 + (p_{\text{c}} - \Delta_{\text{c}})(3p_{\text{c}} - \Delta_{\text{c}})}. \tag{6}$$

Note that $(3p_{\text{c}} - \Delta_{\text{c}}) > 0$, i.e., the laser must be on the blue side of the Kerr-shifted resonance, for symmetry breaking to be observed [25]. Furthermore, the region where the denominator (and hence both derivatives) is negative corresponds to the unstable symmetric solution between the two critical points, shown as a faint green line in Fig. 1(b). Although these formulae hold for the unstable symmetric solution, they are not of much practical use there since the system will always choose one of the two symmetry-broken stable solutions. For these, we must use Eqs. (S1) and (S2) in Supplement 1, which apply in the general asymmetric case. Note that for symmetry-broken states or under asymmetric pumping conditions, the partial derivatives of p_{d} with respect to Δ_{c} and $\tilde{p}_{\text{c}}$ are generally also non-zero [see Eqs. (S3) and (S4) in Supplement 1]. Since the responsivities of p_{d} to Δ_{d} and $\tilde{p}_{\text{d}}$ diverge at the same rate, the pump-power-noise-limited rotation sensitivity does not change significantly when approaching the critical point. However, in a system where noise sources downstream of the resonator, such as electronic noise, dominate, the signal-to-noise ratio will increase with the increased responsivity of the resonator.

A full analysis [37] shows that very close to the critical point the dynamics are governed to leading order by the equation

$$\dot{y} = -y^3 + xy + z, \tag{7}$$

where

$$x = \frac{5p - 2\Delta}{4}\delta_{\text{c}} + \frac{2\Delta - 3p}{4}p\epsilon_{\text{c}},$$

$$y = \sqrt{\frac{15p^2 - 4p\Delta - 4}{8p(3p - \Delta)}}\,p_{\text{d}},$$

$$z = \sqrt{\frac{p(3p - \Delta)(15p^2 - 4p\Delta - 4)}{8}}(\Delta_{\text{d}} + p\epsilon_{\text{d}}), \tag{8}$$

in which $\delta_{\text{c}} = \Delta_{\text{c}} - \Delta$ and Δ_{d} are common-mode (CM) and differential-mode (DM) detuning perturbations, respectively, and ϵ_{c} and ϵ_{d} are CM and DM fractional pump power perturbations, as detailed in Table 1. This tells us that in the steady state ($\dot{y} = 0$) under symmetric pumping conditions ($z = 0$), p_{d} has a square-root dependence on δ_{c} and ϵ_{c} in the symmetry-broken regime ($y = \pm\sqrt{x}$ for $x > 0$ and $y \neq 0$, with $x > 0$, $y = 0$ corresponding to the unstable symmetric state). The differential responsivities of p_{d} to Δ_{d} and ϵ_{d} for the stable states $x < 0$, $y = 0$ and $x > 0$, $y = \pm\sqrt{x}$ may be found from the partial derivative $\partial y/\partial z = 1/(3y^2 - x)$, which is equal to $-1/x$ and $1/(2x)$ in these two cases, respectively, both of which diverge as $x \to 0$. At the critical point itself ($x = 0$), p_{d} has a cube-root steady-state response to Δ_{d} and ϵ_{d} since $y = \sqrt[3]{z}$, while dynamically (specifically in the regime $\lvert z\rvert \gg \lvert y^3 - xy\rvert$) p_{d} behaves as the time integral of Δ_{d} and ϵ_{d}, as we have $\dot{y} \simeq z$. In general, the response of p_{d} to Δ_{d} and ϵ_{d} near the critical point may be characterized as a combination of these proportional, cube-root, and integrator behaviors.

3. EXPERIMENTAL METHODS

The optical circuit used in the experiment is summarized in Fig. 2(a). Light from a narrow-linewidth tunable external-cavity diode laser (ECDL) at around 1550 nm is amplified before being coupled into the microresonator via a tapered optical fiber. Due to the fiber-based nature of the setup, pumping the resonator with the same frequency of light in both directions would have led to a prohibitive problem with interference, depicted in Fig. 2(b). Unavoidable spurious back-reflections from fiber components, connections, etc. would interfere with counterpropagating light, and acoustic and thermal noise in the fibers would cause the relative phase of the interfering waves and, hence, the pump powers seen by the resonator to fluctuate. Even if the back-reflections are at the level of −40 dB, as is typical in our experiment, the pump powers would vary by a few percent, which in our system would limit the rotation sensitivity to around one revolution per second.

To solve this, it was necessary to use different pump frequencies for each direction. Detuning the two pumps by a fraction of the resonator's linewidth and compensating this with a power difference to get back to the critical point [25,37,40] would have helped somewhat, as it would wash out the interference phase at long timescales. However, the resonator still reacts to the percent-level oscillating pump power difference at short timescales, making it impossible for it to stay on average very close to the critical point

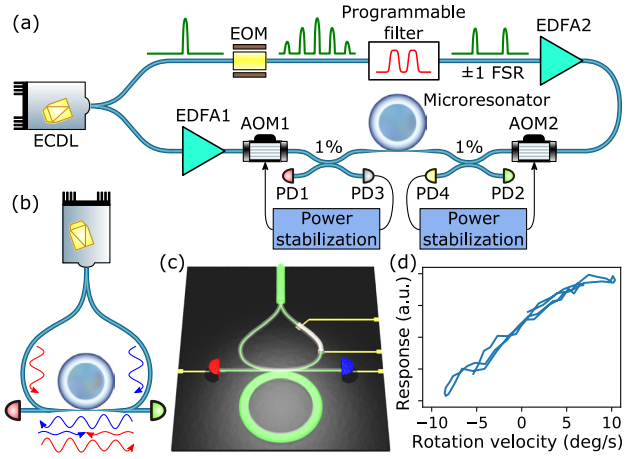

Fig. 2. (a) Optical circuit of the experiment. ECDL, external cavity diode laser; EDFA, erbium-doped fiber amplifier; AOM, acousto-optic modulator; PD, photodiode; FSR, free spectral range (of the microresonator, around 23.7 GHz); 1%, 1% directional coupler. (b) Illustration of the interference effect that prevents us from using the same pump frequency in both directions. (c) Illustration of a possible monolithic chip-based realization of the optical circuit that would not suffer from this interference problem. (d) System response (difference between readings on PD1 and PD2) versus rotation velocity measured using a MEMS gyroscope, indicating a sensitivity of around 2 deg/s.

and exhibit the enormous responsivity enhancement associated with that. To solve this, the two pump frequencies were offset by the resonator's free spectral range (FSR), so that the counterpropagating waves would continue to have near-perfect spatial overlap within the resonator (due to being coupled into the same mode family) and, hence, experience the same Kerr interaction, whilst the interference would be removed completely. This dramatically improves the pump power stabilities, allowing the system to remain much closer to the critical point. However, offsetting the counterpropagating pump frequencies by one FSR makes the system sensitive to temperature-related drifts in the FSR, as these now translate into pump detuning differences. This, in turn, was solved by making one of the pumps an equal composition of light one FSR higher and one FSR lower than the other. As shown in Fig. 2(a), this was achieved by sending the light through an electro-optic modulator (EOM) driven with an RF frequency equal to the FSR, followed by a programmable wavelength filter. This allowed the system to be placed at a point where it is first-order-insensitive to variations in the FSR, which was achieved by fine-tuning the EOM's RF drive frequency until the transmitted powers measured on PD1 and PD2 were locally stationary with respect to the drive frequency. This stationary point occurs when the EOM's drive frequency exactly matches the FSR, which would typically wander by a few Hz over several minutes due to thermal drift of the resonator.

It is worth noting that splitting one pump into two separate frequencies increases its effective self-phase modulation strength by a factor of 3/2, since each frequency experiences a combination of its own self-phase modulation and the twice-as-strong cross-phase modulation from the other frequency. A full quantitative treatment of this situation is presented in [37], which shows how the critical point can be attained by compensating this imbalance through pump power and/or detuning differences [40]. However, this does not significantly change the critical dynamics so that Eq. (2) still holds.

It is important to stress that these somewhat convoluted measures for overcoming the interference problem are likely not to be needed if the optical circuit is realized on a monolithic chip-based platform [illustrated in Fig. 2(c)], as is the aim for this gyroscope. This is because the very short optical paths and monolithic nature of the setup would ensure that the phase of any interference remains extremely stable, meaning that both pumps can have the same frequency without their powers fluctuating significantly.

Turning again to our setup [Fig. 2(a)], the pump powers were monitored using PD3 and PD4 and continuously stabilized by feeding back to the amplitudes of the RF signals driving the acousto-optic modulators (AOMs), AOM1 and AOM2. The frequencies of the RF signals to the AOMs were used to control the pump detuning difference between the two directions in order to tune the system to the critical point. The transmitted powers were recorded via PD1 and PD2. Rotation of the resonator was achieved by mounting the entire optical circuit except for the laser and erbium-doped fiber amplifier EDFA1, plus some of the electronics, on a structure suspended from the ceiling that acted as a torsional pendulum. Light was transmitted to this part of the setup via polarization-maintaining (PM) fibers and linear polarizers to ensure that the incoming polarizations remained constant as the setup was rotated. Although most fibers on the rotating setup itself were non-PM, care was taken to minimize the effect of polarization drift on the pump powers seen by the (polarization-sensitive) resonator. This was done by filtering the polarization just before the pick-offs to PD3 and PD4, by minimizing lengths of fiber and by securing any loose sections of fiber. Fiber polarization controllers were placed immediately before each polarization-sensitive element of the circuit. A third pick-off (1% directional coupler) was placed just after the programmable filter to allow the spectrum to be monitored on an optical spectrum analyzer. Around 50 mW of optical power was sent into the tapered fiber in each direction.

The angular velocity of the rotating setup was detected using a chip-based MEMS gyroscope mounted rigidly to it. This was used to produce Fig. 2(d), in which the difference between the transmitted powers measured on PD1 and PD2—the "response"—was recorded alongside the MEMS gyroscope reading as the torsional pendulum setup rotated freely back and forth a few times over the course of 42 s. This measurement indicates a rotation sensitivity of around 2 deg/s, which is limited by the accuracy with which the pump powers seen by the resonator are able to be stabilized due to various sources of noise in the setup. The resonator's enhancement factor $\partial p_d/\partial \Delta_d$ in this measurement was around 10^4.

To characterize the dynamical response of the system, it was necessary to perform extended measurements under rapidly varying angular velocity. Since the torsional pendulum was hand-actuated, rather than physically rotating the setup in these measurements, we simulated a time-dependent Sagnac splitting by varying the pump detuning difference Δ_d via the AOM drive frequencies. As well as giving better control over the Sagnac splitting and allowing overnight automated measurements, this avoided potential systematic errors from slight deformations to the setup caused by inertial forces. At these larger angular accelerations, such deformations might have perturbed the pump powers seen by the resonator enough to significantly affect the rotation measurements. In fact, since in the region very close to the critical point but just outside the symmetry-broken regime the system is much more sensitive to Δ_d than to Δ_c, this effect could be achieved by varying just one of the AOM frequencies. Although this would cause both the DM

and CM detunings Δ_d and Δ_c to change, the effect of the variation in Δ_c was negligible. This can be seen from Eq. (7) by noting that in the steady state ($\dot{y} = 0$)

$$\frac{\partial y}{\partial x} = y\frac{\partial y}{\partial z}, \tag{9}$$

and that $|y| \ll 1$ very close to the critical point. Furthermore, variations in Δ_c are heavily suppressed at timescales of more than $\sim$10 μs as a result of the strong thermal nonlinearity of the silica resonator [41]. After adjusting the laser frequency and detuning difference to reach the critical point (judged by manually modulating the detuning difference back and forth by $\sim$10 Hz and maximizing the perceived responsivity $\partial p_d/\partial \Delta_d$ when observing the two transmitted powers on an oscilloscope), we waited a few minutes for the resonator to thermalize. Next, all of the polarizations were optimized, and the EOM frequency was tuned to the aforementioned stationary point, after which the RF frequency to AOM1 was modulated sinusoidally at 500 Hz, and a lock-in measurement of the system's response to this was made. This measurement was performed for a range of both Δ_c (accessed via the laser frequency) and the DC offset of Δ_d (accessed via the DC offset to the driving frequency of AOM1) over the course of several hours. To compensate for any thermal drift in the FSR that would take the system away from the stationary point, the EOM frequency was automatically adjusted back to this point at regular intervals. This was achieved by modulating it at 10 kHz, performing an in-phase lock-in measurement of the system's response, and stabilizing this to zero by feeding back to the EOM frequency's DC offset, before turning off the modulation and retaining the offset's last value.

The readings on PD1 and PD2 were converted to the dimensionless quantities $p_{1,2}$ by the following procedure: firstly, quantities proportional to $p_{1,2}$, which shall be referred to as "coupled powers," were calculated as the differences between the PD readings and their "baseline values" taken when the pump was completely out of resonance. Next, the value of $p/\tilde{p}$ at the critical point was calculated as the mean of the two ratios $p_{1,2}/\tilde{p}_{1,2}$ between the coupled powers at the critical point and at maximum coupling (when the pump is perfectly on resonance and $p_{1,2} = \tilde{p}_{1,2}$). This was then used to find p (along with Δ) at the critical point by combining Eqs. (3) and (4), thus giving the constants of proportionality between the coupled powers and $p_{1,2}$.

Values of Δ_d were found by dividing the detuning difference offset from the critical point by twice the cavity half-linewidth γ, which was measured using a cavity ringdown technique [42] to be around $2\pi \times 330$ kHz. Furthermore, time and angular frequency of modulation are normalized by $1/\gamma$ and γ, respectively. Importantly, the thermal shift of the resonance frequencies in silica resonators is huge [41], at almost two orders of magnitude larger than the Kerr shift. This meant that Δ_c, or its offset δ_c from the critical point, could not be obtained directly from the laser frequency. Instead, they were calculated from p_c and the critical point values p and Δ via the relation $\partial p_c/\partial \Delta_c = 1/4$ that holds at the critical point. The strong thermal nonlinearity did not have a significant effect on the critical dynamics, as it only interacts with Δ_c and not Δ_d, to which the system is much more sensitive [see Eq. (9)], and which we are interested in measuring. In fact, it served to suppress fluctuations in Δ_c coming from laser frequency excursions of the order of a few megahertz (MHz), greatly stabilizing the gain of the system.

4. RESULTS AND DISCUSSION

Figure 3(a) shows the DM circulating power p_d versus the CM detuning offset δ_c from the critical point, for six downward sweeps of the laser frequency across the critical point. Note that p_d randomly chooses one sign or the other during each sweep as the detuning passes the critical point. These are overlaid with the stable steady-state solutions to Eq. (7) for $z = 0$, namely, $y = 0$ for $x < 0$ and $y = \pm\sqrt{x}$ for $x > 0$. The scaling factors from x and y to δ_c and p_d are calculated from the experimentally determined values of $p = 1.02$ and $\Delta = 1.85$ at the critical point via Eq. (8). The fact that the curvature of the parabola matches the data without fitting provides validation for the model. The slight deviations from the theory far from the critical point are due to the fact that the system is not truly symmetric because of the difference in the effective self-phase-modulation coefficients for the counterpropagating directions, as discussed in Section 3. For values of $|\delta_c|$ of order 1, the system begins to deviate noticeably from the universal behavior governed by Eq. (7) and manifest this underlying asymmetry. The dashed rectangle in Fig. 3(a) indicates the region shown in Figs. 3(b)–3(g).

Figures 3(b)–3(d) depict the system's measured response to a sinusoidally modulated DM detuning offset

$$\Delta_d = \Delta_d^{DC} + \Delta_d^{AC}\cos(\Omega_{mod}t), \tag{10}$$

where Δ_d^{AC} and Ω_{mod} are 8.4×10^{-4} and 1.5×10^{-3}, respectively, in dimensionless units. Each data point represents a measurement lasting 100 ms, or 50 periods of the modulation, from which the time averages of both the DC and demodulated DM circulating power,

$$p_d^{DC} = \langle p_d \rangle \quad \text{and} \quad p_d^{AC} = 2\langle p_d e^{i\Omega_{mod}t}\rangle, \tag{11}$$

respectively, were obtained. Throughout the measurement period, the laser frequency was scanned with a 0.1 Hz triangle wave over a range of more than 100 MHz (due to the large thermal nonlinearity of silica discussed at the end of Section 3 [41]) to access a range of CM detunings δ_c. The value of δ_c for each data point was derived from the time-averaged measured value of p_c, as discussed at the end of Section 3. After every 1000 data points, the value of the DC DM detuning Δ_d^{DC} was changed and was cycled in this way through 70 values evenly spaced in the range $\pm 4 \times 10^{-3}$.

The magnitude and phase of p_d^{AC}, as well as Δ_d^{DC}, are represented by the colors of the data points in Figs. 3(b)–3(d), respectively, in all of which the horizontal and vertical coordinates are δ_c and p_d^{DC}, respectively. The reason why p_d^{DC} rather than the independent variable Δ_d^{DC} is used as the vertical axis is because there is noise on the pump power difference that has a very similar effect to noise on Δ_d^{DC}. Even though this noise is at the level of 10^{-4}, it is significant in this measurement since the system's responsivities to fractional differences in pump power and to differences in normalized detuning are roughly equal, as can be seen from the expression for z in Eq. (8). Despite all the steps taken to reduce relative pump power fluctuations in the setup, there were still a few sources of this noise. Plotting the data in this way allows the effects of this noise to be excluded from Figs. 3(b) and 3(c).

From Fig. 3(b), we can see a dramatic increase in the responsivity around the critical point, which is a universal feature of critical dynamics. From Fig. 3(c), we observe a phase lag in the AC response approaching $\pi/2$, which shows that the system is acting more like an integrator than a proportional amplifier. This

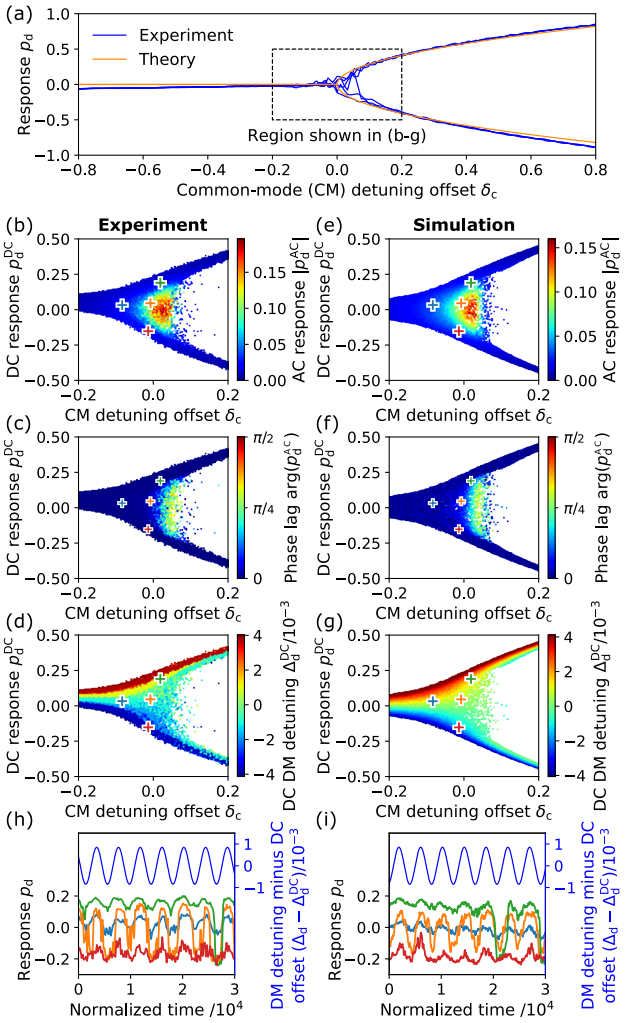

Fig. 3. (a)–(d), (h) Experimental results with (a) theoretical curves and (e)–(g), (i) simulations based on our simplified critical dynamics model with no free parameters. All quantities are given in their dimensionless forms [see Table 1 and Eqs. (10) and (11)]. (a) DM circulating power p_d versus CM detuning offset δ_c from the critical point for six sweeps of the laser frequency, showing the symmetry breaking in either direction, with theoretical curves overlaid. (b), (e) Magnitude and (c), (f) phase of the demodulated AC response p_d^{AC} to a sinusoidally modulated rotation at 500 Hz ($\Omega_{mod} = 2\pi \times 500\,\mathrm{Hz}/\gamma = 1.5 \times 10^{-3}$ in dimensionless units) versus CM detuning offset δ_c and DC response p_d^{DC} for a range (d), (g) of DM detuning DC offsets Δ_d^{DC}. Rather than physically rotating the setup, the detuning difference between the pumps was modulated via the RF frequency to AOM1 (see Fig. 1) to mimic the Sagnac splitting. The (half-peak-to-peak) modulation amplitude was 560 Hz or $\Delta_d^{AC} = 2\pi \times 560\,\mathrm{Hz}/(2\gamma) = 8.4 \times 10^{-4}$ in dimensionless units [the factor of 2 on the denominator coming from $\Delta_d = (\Delta_1 - \Delta_2)/2$ and the fact that the sinusoidal modulation is only applied to Δ_1], which corresponds to 23 deg/s of rotation velocity. (h), (i) System response p_d versus time (normalized by the inverse half-linewidth $1/\gamma$) for four different sets of parameters δ_c and Δ_d^{DC} indicated by correspondingly colored crosses in (b)–(g), alongside the input modulation signal $\Delta_d - \Delta_d^{DC}$.

is a clear indicator of critical slowing down, another universal critical behavior [32]. Although it is responsible, together with the aforementioned noise, for limiting the maximum AC responsivity, it also causes the resonator to integrate the rotation velocity signal with respect to time, which could be useful, for example, for inertial navigation.

The data for Δ_d^{DC} versus δ_c and p_d^{DC} [Fig. 3(d)] were fitted with a theoretical function based on the steady-state solution to Eq. (7), and the residuals of this fit versus time were then used to find the frequency spectrum of the equivalent noise on Δ_d^{DC}. As expected, due to the multiple sources of noise, the power spectral density (PSD) has an approximate overall $1/f$ dependency; a fit of this function to the PSD versus frequency (on a log-log plot) gives a coefficient of 1.5×10^{-9} in units of Δ_d^2, which in our setup is equivalent to an rms noise on the measured rotation velocity of around 0.25 deg/s/$\sqrt{\mathrm{Hz}}$ at 1 kHz. The measurement noise in units of Δ_d is approximately equal to the noise on the DM fractional pump power ϵ_d and can be reduced by moving to a monolithic chip-based waveguide circuit, as illustrated in Fig. 2(c). On such a platform, the pump power difference and polarizations would be passively stable, rather than relying on separate feedback circuits and polarization filters for each direction. In addition, the orders-of-magnitude-lower path length noise would mean that interference from back-reflections [see Fig. 2(b)] would not lead to significant pump power fluctuations, and thus the same pump frequencies could be used in both directions, greatly simplifying the circuit. The only active element that would be required in the optical circuit would be a variable attenuator for fine-tuning the balance between the two pump powers, which could be based on any of a number of electro-optic or thermo-optic effects. Furthermore, for a given noise level in units of Δ_d, the noise level on the measured rotation velocity can be reduced by increasing the Q factor or diameter of the resonator, as can be seen from Eq. (1) and the relation $\Delta\omega = 2\gamma\Delta_d$, where $\Delta\omega$ is the Sagnac splitting referred to in Eq. (1).

Figure 3(h) shows some traces of p_d versus dimensionless time γt for the different values of δ_c and p_d^{DC}, alongside the sinusoidal modulation curve of Δ_d with the DC offset removed. The greatly increased gain of the system, both to the sinusoidal modulation of Δ_d and to the noise on p_d, near the critical point is apparent by comparing the traces. Note also how for the green trace, which occurs just inside the symmetry-broken region, a relatively large excursion in the noise that coincides with the correct part of the modulation cycle can cause p_d to switch momentarily from one symmetry-broken state to the other.

Figures 3(e)–3(g), 3(i) show the correponding results of a simulation of Eq. (7) with the same parameters as in the experiment, with the scaling factors between the dimensionless experimental variables and x, y and z calculated using Eq. (8). In the simulation, $1/f$ noise was added to the sinusoidally modulated input variable z with the same coefficient as was obtained from the fit to the experimental noise spectrum. The experimental and simulated plots agree well, with any discrepancy originating from uncertainty in the measured values of parameters such as γ, as well as from the slight asymmetry of the system due to the two pump frequencies being sent in one of the directions (see Section 3). The switching events seen on the green traces in Figs. 3(h) and 3(i) are responsible for the sparse scattering of points to the right of the center in Figs. 3(b)–3(d) and 3(e)–3(g); the occurrence of a similar number of these outliers in the experimental and simulated data lends support to the $1/f$ noise model.

5. CONCLUSION AND OUTLOOK

We have demonstrated a proof-of-principle nonlinear enhanced microresonator gyroscope that operates at the critical point of

Kerr-induced symmetry breaking between counterpropagating light in a bidirectionally pumped ring resonator. Rotation in the plane of the microresonator causes a tiny "seed" splitting between the counterpropagating resonance frequencies due to the Sagnac effect, which is then amplified by four orders of magnitude via a positive feedback cycle between resonance splittings and circulating power differences. It can then be "read off" from the microresonator as a large difference between the in-coupled powers in the two directions.

In addition to demonstrating rotation measurement with a sensitivity of around 2 deg/s, we have characterized the dynamical response of the system to a sinusoidally varying simulated rotation generated by modulating the pump detuning difference. These measurements were shown, via a numerical simulation, to be well described by a simple theoretical model for the system's critical dynamics [37] and provide direct evidence for two universal critical behaviors, namely, responsivity enhancement and critical slowing down.

At the critical point, the system exhibits divergent responsivity not only to rotation, which is equivalent to pump detuning differences between the two directions, but also to pump power differences. This is similar to the well-known issue with EP-based sensors, where various noise sources are amplified by the same factor as the signal [15–18]. It means that in order to achieve a certain rotation sensitivity, it is necessary to stabilize the pump power difference to an equally high degree, since the system responds about equally to a certain fractional pump power difference as it does to a Sagnac splitting that is the same fraction of the linewidth. We believe that by moving to a monolithic chip-based platform with waveguide circuits and resonators, differential pump power stabilities orders of magnitude higher than in this experiment could be achieved passively. In addition, by increasing the Q factor and/or diameter of the resonator, rotation sensitivities approaching those of today's FOGs or RLGs could be achieved in a simple device with a fraction of the size, weight, power consumption, and cost.

Funding. Royal Academy of Engineering (ICRF1718\1\52); Horizon 2020 Framework Programme (756966); H2020 Marie Skłodowska-Curie Actions (GA-2015-713694, 748519); Engineering and Physical Sciences Research Council.

Acknowledgment. J. M. S. was supported by the Royal Academy of Engineering and the Office of the Chief Science Adviser for National Security under the UK Intelligence Community Postdoctoral Fellowship Programme. L. D. B. and M. T. M. W. acknowledge funding from EPSRC through the Centre for Doctoral Training in Applied Photonics. A. Ø. S. acknowledges funding from the Aker Scholarship and from EPSRC through the Quantum Systems Engineering Programme.

Disclosures. The authors declare no conflicts of interest.

Data availability. Data underlying the results presented in this paper are not publicly available at this time but may be obtained from the authors upon reasonable request.

Supplemental document. See Supplement 1 for supporting content.

REFERENCES

1. F. Dell'Olio, T. Tatoli, C. Ciminelli, and M. N. Armenise, "Recent advances in miniaturized optical gyroscopes," J. Eur. Opt. Soc. Publ. **9**, 14013 (2014).
2. H. L. Ma, J. J. Zhang, L. L. Wang, and Z. H. Jin, "Development and evaluation of optical passive resonant gyroscopes," J. Lightwave Technol. **35**, 3546–3554 (2017).
3. E. J. Post, "Sagnac effect," Rev. Mod. Phys. **39**, 475–493 (1967).
4. H. Ma, J. Zhang, L. Wang, and Z. Jin, "Double closed-loop resonant micro optic gyro using hybrid digital phase modulation," Opt. Express **23**, 15088–15097 (2015).
5. J. Wang, L. Feng, Y. Tang, and Y. Zhi, "Resonator integrated optic gyro employing trapezoidal phase modulation technique," Opt. Lett. **40**, 155–158 (2015).
6. W. Liang, V. S. Ilchenko, A. A. Savchenkov, E. Dale, D. Eliyahu, A. B. Matsko, and L. Maleki, "Resonant microphotonic gyroscope," Optica **4**, 114–117 (2017).
7. J. Li, M.-G. Suh, and K. Vahala, "Microresonator Brillouin gyroscope," Optica **4**, 346–348 (2017).
8. Y.-H. Lai, Y.-K. Lu, M.-G. Suh, Z. Yuan, and K. Vahala, "Observation of the exceptional-point-enhanced Sagnac effect," Nature **576**, 65–69 (2019).
9. Y.-H. Lai, M.-G. Suh, Y.-K. Lu, B. Shen, Q.-F. Yang, H. Wang, J. Li, S. H. Lee, K. Y. Yang, and K. Vahala, "Earth rotation measured by a chip-scale ring laser gyroscope," Nat. Photonics **14**, 345–349 (2020).
10. J. J. Wang, L. S. Feng, Q. W. Wang, H. C. Jiao, and X. Wang, "Suppression of backreflection error in resonator integrated optic gyro by the phase difference traversal method," Opt. Lett. **41**, 1586–1589 (2016).
11. P. P. Khial, A. D. White, and A. Hajimiri, "Nanophotonic optical gyroscope with reciprocal sensitivity enhancement," Nat. Photonics **12**, 671 (2018).
12. H. Zhang, J. M. Liu, J. Lin, W. X. Li, X. Xue, A. P. Huang, and Z. S. Xiao, "On-chip tunable dispersion in a ring laser gyroscope for enhanced rotation sensing," Appl. Phys. A **122**, 501 (2016).
13. J. Ren, H. Hodaei, G. Harari, A. U. Hassan, W. Chow, M. Soltani, D. Christodoulides, and M. Khajavikhan, "Ultrasensitive micro-scale parity-time-symmetric ring laser gyroscope," Opt. Lett. **42**, 1556–1559 (2017).
14. S. Sunada, "Large Sagnac frequency splitting in a ring resonator operating at an exceptional point," Phys. Rev. A **96**, 033842 (2017).
15. W. Langbein, "No exceptional precision of exceptional-point sensors," Phys. Rev. A **98**, 023805 (2018).
16. H.-K. Lau and A. A. Clerk, "Fundamental limits and non-reciprocal approaches in non-Hermitian quantum sensing," Nat. Commun. **9**, 1–13 (2018).
17. H. Wang, Y.-H. Lai, Z. Yuan, M.-G. Suh, and K. Vahala, "Petermann-factor sensitivity limit near an exceptional point in a Brillouin ring laser gyroscope," Nat. Commun. **11**, 1610 (2020).
18. M. Zhang, W. Sweeney, C. W. Hsu, L. Yang, A. D. Stone, and L. Jiang, "Quantum noise theory of exceptional point amplifying sensors," Phys. Rev. Lett. **123**, 180501 (2019).
19. J. Wiersig, "Robustness of exceptional-point-based sensors against parametric noise: the role of Hamiltonian and Liouvillian degeneracies," Phys. Rev. A **101**, 053846 (2020).
20. P. Del'Haye, A. Schliesser, O. Arcizet, T. Wilken, R. Holzwarth, and T. J. Kippenberg, "Optical frequency comb generation from a monolithic microresonator," Nature **450**, 1214–1217 (2007).
21. B. Stern, X. C. Ji, Y. Okawachi, A. L. Gaeta, and M. Lipson, "Battery-operated integrated frequency comb generator," Nature **562**, 401 (2018).
22. S. Zhang, J. M. Silver, L. D. Bino, F. Copie, M. T. M. Woodley, G. N. Ghalanos, A. Ø. Svela, N. Moroney, and P. Del'Haye, "Sub-milliwatt-level microresonator solitons with extended access range using an auxiliary laser," Optica **6**, 206–212 (2019).
23. L. Del Bino, J. M. Silver, S. L. Stebbings, and P. Del'Haye, "Symmetry breaking of counter-propagating light in a nonlinear resonator," Sci. Rep. **7**, 43142 (2017).
24. Q. T. Cao, H. M. Wang, C. H. Dong, H. Jing, R. S. Liu, X. Chen, L. Ge, Q. H. Gong, and Y. F. Xiao, "Experimental demonstration of spontaneous chirality in a nonlinear microresonator," Phys. Rev. Lett. **118**, 033901 (2017).
25. M. T. M. Woodley, J. M. Silver, L. Hill, F. Copie, L. Del Bino, S. Y. Zhang, G. L. Oppo, and P. Del'Haye, "Universal symmetry-breaking dynamics for the Kerr interaction of counterpropagating light in dielectric ring resonators," Phys. Rev. A **98**, 053863 (2018).
26. L. Del Bino, J. M. Silver, M. T. M. Woodley, S. L. Stebbings, X. Zhao, and P. Del'Haye, "Microresonator isolators and circulators based on the intrinsic nonreciprocity of the Kerr effect," Optica **5**, 279–282 (2018).
27. B. A. Daniel and G. P. Agrawal, "Phase-switched all-optical flip-flops using two-input bistable resonators," IEEE Photon. Technol. Lett. **24**, 479–481 (2012).

28. A. E. Kaplan and P. Meystre, "Enhancement of the Sagnac effect due to nonlinearly induced nonreciprocity," Opt. Lett. **6**, 590–592 (1981).
29. C. Wang and C. P. Search, "Enhanced rotation sensing by nonlinear interactions in silicon microresonators," Opt. Lett. **39**, 4376–4379 (2014).
30. C. Wang and C. P. Search, "A nonlinear microresonator refractive index sensor," J. Lightwave Technol. **33**, 4360–4366 (2015).
31. A. Ø. Svela, J. M. Silver, L. Del Bino, G. Ghalanos, N. Moroney, M. T. Woodley, S. Zhang, M. Vanner, and P. Del'Haye, "Spontaneous symmetry breaking based near-field sensing with a microresonator," in *Conference on Lasers & Electro-optics (CLEO): QELS_Fundamental Science* (Optical Society of America, 2019), paper JM3B-3.
32. H. E. Stanley, *Phase Transitions and Critical Phenomena* (Clarendon, 1971).
33. P. W. Higgs, "Broken symmetries and the masses of gauge bosons," Phys. Rev. Lett. **13**, 508–509 (1964).
34. J. Bardeen, L. N. Cooper, and J. R. Schrieffer, "Theory of superconductivity," Phys. Rev. **108**, 1175–1204 (1957).
35. L. Landau, "Theory of the superfluidity of helium II," Phys. Rev. **60**, 356 (1941).
36. P. Del'Haye, S. A. Diddams, and S. B. Papp, "Laser-machined ultra-high-Q microrod resonators for nonlinear optics," Appl. Phys. Lett. **102**, 221119 (2013).
37. J. M. Silver, K. T. Grattan, and P. Del'Haye, "Critical dynamics of an asymmetrically bidirectionally pumped optical microresonator," arXiv:1912.08262 (2019).
38. H. Lee, T. Chen, J. Li, K. Y. Yang, S. Jeon, O. Painter, and K. J. Vahala, "Chemically etched ultrahigh-Q wedge-resonator on a silicon chip," Nat. Photonics **6**, 369–373 (2012).
39. V. M. N. Passaro, A. Cuccovillo, L. Vaiani, M. De Carlo, and C. E. Campanella, "Gyroscope technology and applications: a review in the industrial perspective," Sensors **17**, 2284 (2017).
40. B. Garbin, J. Fatome, G.-L. Oppo, M. Erkintalo, S. G. Murdoch, and S. Coen, "Asymmetric balance in symmetry breaking," Phys. Rev. Res. **2**, 023244 (2020).
41. T. Carmon, L. Yang, and K. J. Vahala, "Dynamical thermal behavior and thermal self-stability of microcavities," Opt. Express **12**, 4742–4750 (2004).
42. C. Lecaplain, C. Javerzac-Galy, M. L. Gorodetsky, and T. J. Kippenberg, "Mid-infrared ultra-high-Q resonators based on fluoride crystalline materials," Nat. Commun. **7**, 13383 (2016).